# $Co/Co_9S_8$@Carbon Nanotubes on Carbon Sheet: Facile Controlled Synthesis, Electrocatalysis on Oxygen Reduction Reaction/Oxygen Evolution Reaction, and Application on Rechargeable Zn-air Battery

Han-Ming Zhang, † [a,b] Chunyan Hu, † [b] Muwei Ji,*[b] Minjie Wang,[b] Jiali Yu,[b] Huichao Liu,[b] Caizhen Zhu,*[b] and Jian Xu[b]

a. Hebei Key Laboratory of Material Near-Net Forming Technology, School of Materials Science and Engineering, Hebei University of Science and Technology, Shijiazhuang, 050018, P. R. China.

b. Institute of Low-dimensional Materials Genome Initiative, College of Chemistry and Environmental Engineering, Shenzhen University, Shenzhen, Guangdong, 518060, P. R. China.

† The authors contributed equally in this work.

Corresponding Author:

jimuwei@163.com (Muwei Ji)

czzhu@szu.edu.cn (Caizhen Zhu).

# Experiment：

**ORR test:** The ORR polarization curves were measured at predefined rotation rates and a scan rate of 10 mV $s^{-1}$ in $O_2$ and $N_2$-saturated 0.1 M KOH electrolyte for deduction background. The 5000 potential cycles of the optimal catalyst were tested in $O_2$-saturated 0.1 M KOH electrolyte at a scan rate of 50 mV $s^{-1}$ (0.2-1.0 V vs. RHE) for ORR long term durability test.

Based on the RRDE measurement, the change of n values per oxygen molecule in oxygen reduction can also be calculated according to Equation (1), and the corresponding generation rates of $H_2O_2$ can be calculated according to Equation (2):

$$n = 4 \times \frac{|I_d|}{|I_d| + I_r/N} \quad \text{Equation (1)}$$

$$H_2O_2\% = 200 \times \frac{I_r/N}{|I_d| + I_r/N} \quad \text{Equation (2)}$$

where $I_d$ is the disk current, Ir is the ring current, and N is the current collection efficiency of Pt ring. N was calculated to be 0.37 for the reduction of $K_3Fe(CN)_6$.

**OER test:** The OER polarization curves were measured with a scan rate of 5.0 mV $s^{-1}$ at room temperature in $N_2$ and $O_2$-saturated 1.0 M KOH, respectively. Before OER polarization curve tests, the cyclic voltammetry was tested with a scan rate of 50 mV $s^{-1}$ for OER (1.0-1.9 V vs. RHE), respectively.

All potentials were auto iR-compensated. The diameter of the rotating disk electrode (RDE) with a glassy carbon disk was 5 mm, which was used as the substrate for the working electrode. In the whole measurement, the Ag/AgCl-saturated KCl electrode was used as the reference electrode. The counter electrode was a Pt wire in the ORR and OER measurement.

The measured potentials were converted to the reversible hydrogen electrode (RHE) using the following Equation (3):

$$V_{RHE} = V_{Ag/AgCl} + V^{o}_{Ag/AgCl} + 0.059\, pH \qquad \text{Equation (3)}$$

where $V^{0}_{Ag/AgCl}$ was 0.197 V at room temperature and pH is 13 of 0.1 M KOH, and 14 of 1.0 M KOH.

**Aqueous Zn-air Battery Measurements:** The homemade air cathode consisted of $Co/Co_9S_8$@CNTs-900 catalyst layer on the gas diffusion layer. The loading of catalyst is 2 mg $cm^{-2}$. For comparison, air cathode equipped with the same loading of 20 wt% Pt/C and $RuO_2$ (mass ratio 1:1) catalyst was also tested. A polished Zn plate with a thickness of 0.05 mm was used as the anode.

Figure S1 to S

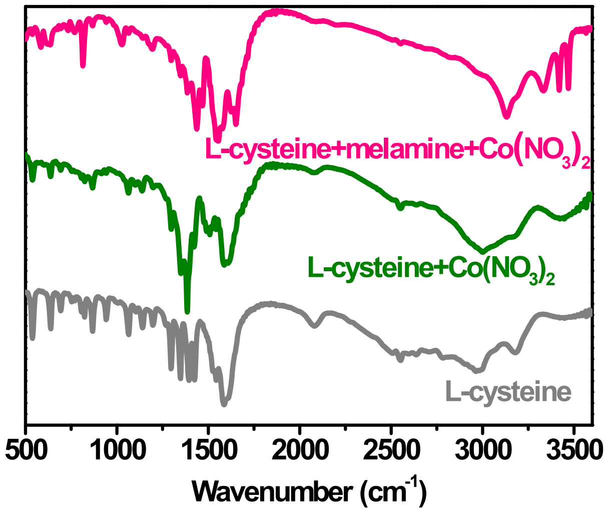


**Figure S1.** FTIR spectrum of the original L-cysteine (gray line); the mixture of L-cysteine and $Co(NO_3)_2$ (green line); the mixture of L-cysteine, melamine and $Co(NO_3)_2$ after grinding for 20 min. The FTIR spectrum shows that vibration of L-cysteine change obviously. The peaks around 1300 $cm^{-1}$ become weaker and a new peak at 1384 $cm^{-1}$ produces, which illustrate the coordination of $Co^{2+}$ and L-cysteine.

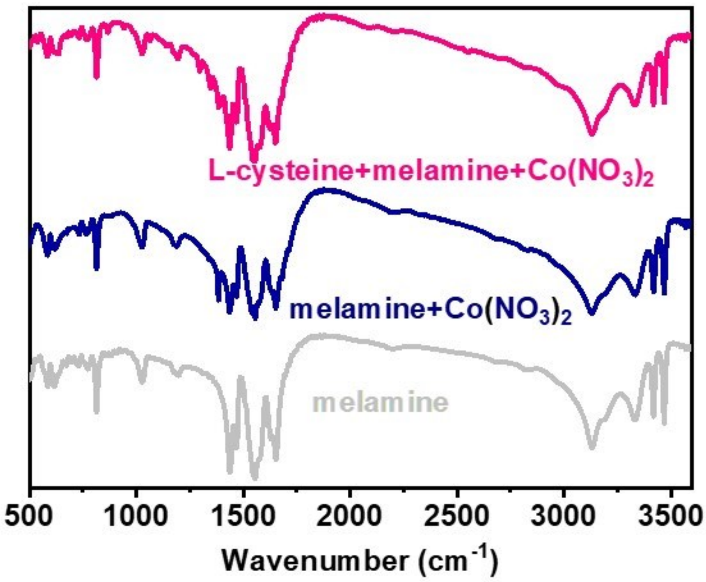


**Figure S2.** FTIR spectrum of the original melamine, melamine+ $Co(NO_3)_2$ and L-cysteine+melamine+$Co(NO_3)_2$. The FTIR spectrum shows that after grinding with $Co(NO_3)_2$, the vibration of melamine remain well, which reveal that the melamine is inert to $Co(NO_3)_2$ and no coordination occurs.

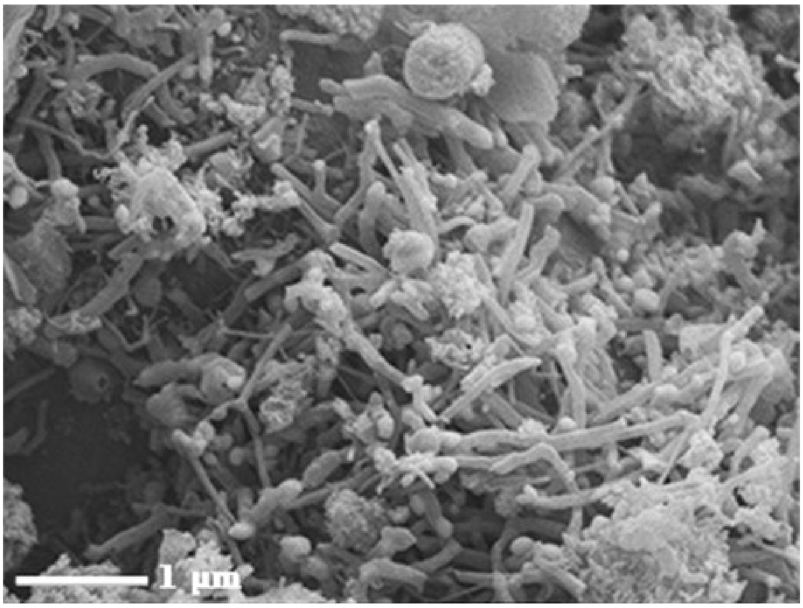


**Figure S3.** FE-SEM images of $Co/Co_9S_8$@CNTs-900.

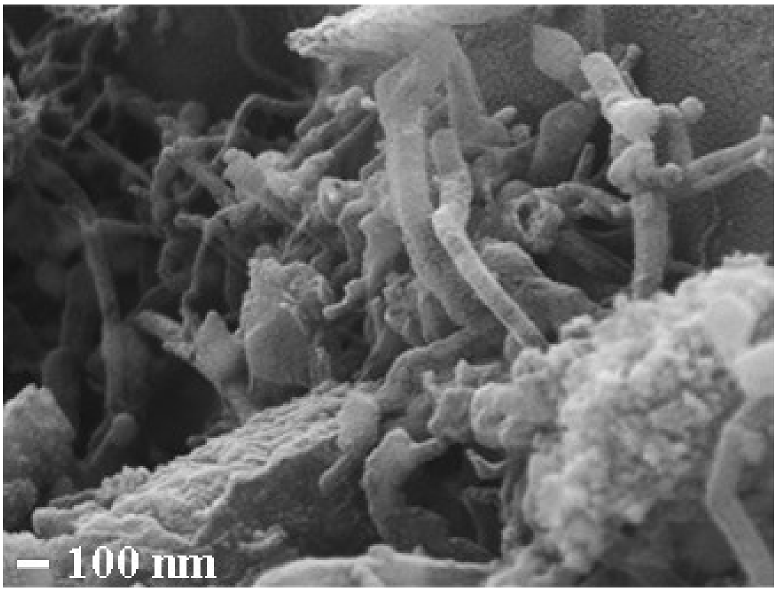


**Figure S4.** SEM image of $Co/Co_9S_8$@CNTs-800.

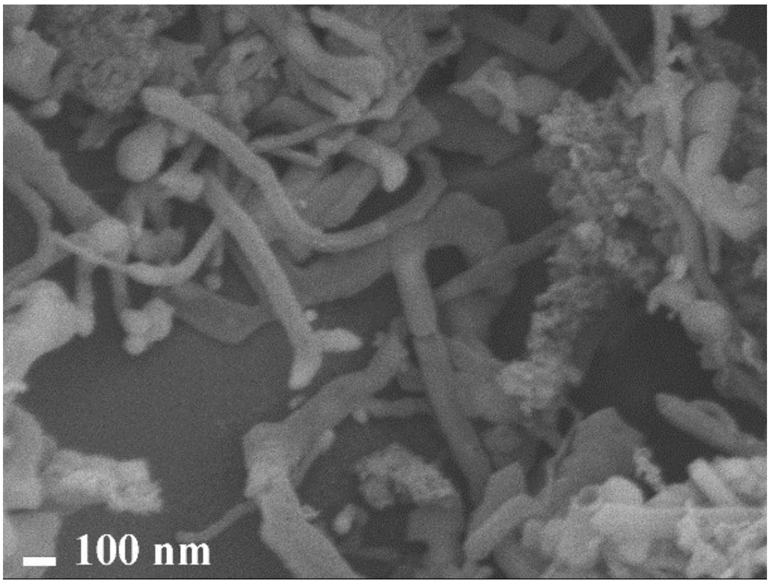


**Figure S5.** SEM image of Co/$Co_9S_8$@CNTs-1000.

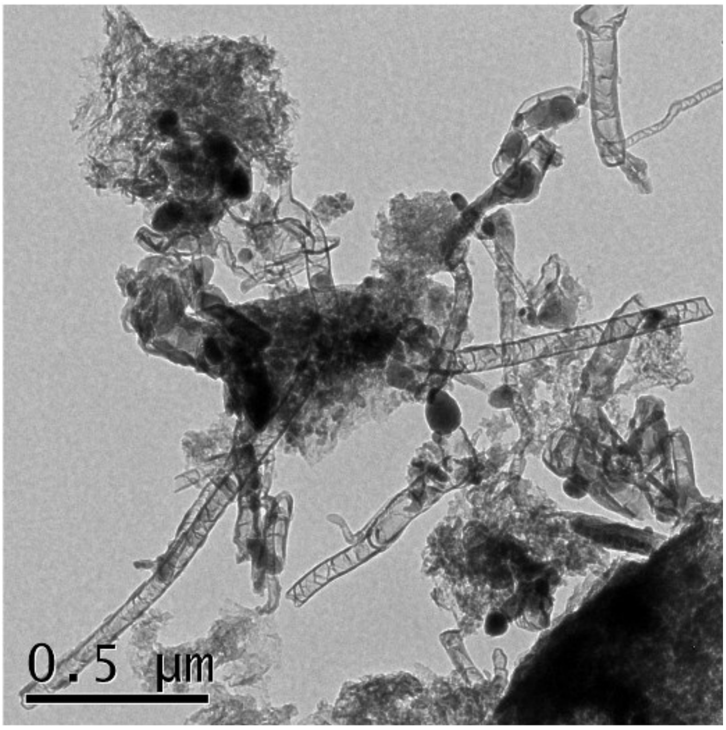


**Figure S6.** TEM images of Co/$Co_9S_8$@CNTs-900.

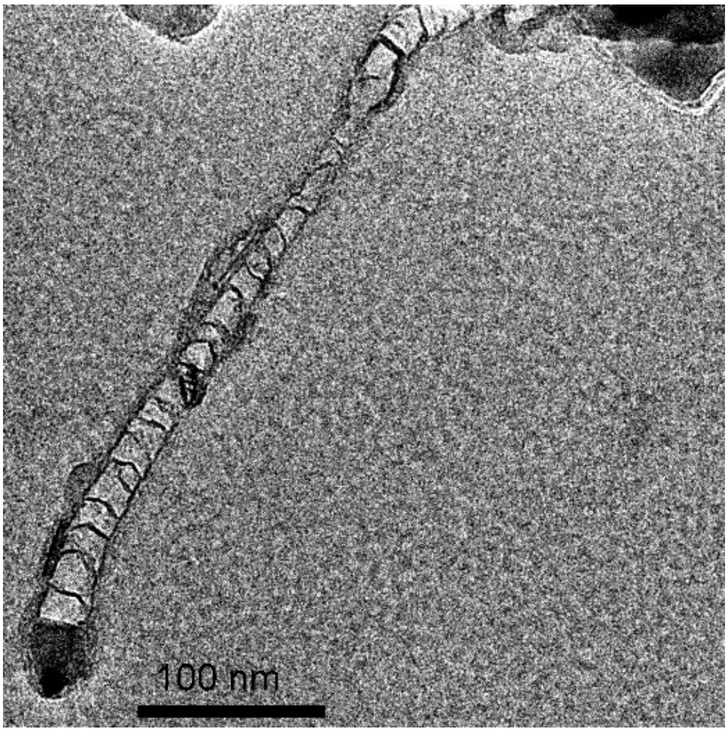


**Figure S7.** TEM images of Co/$Co_9S_8$@CNTs-800.

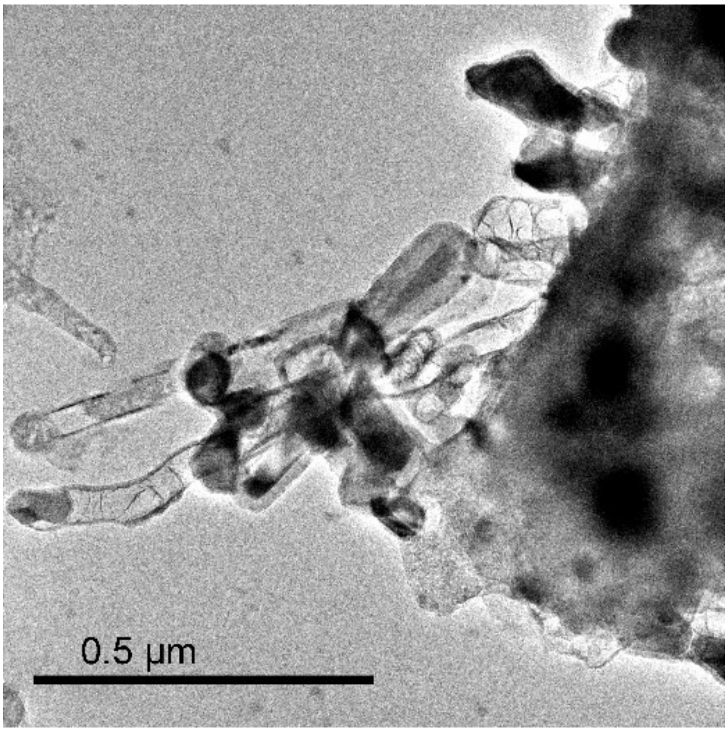


**Figure S8.** TEM images of Co/$Co_9S_8$@CNTs-1000.

**Table S1.** Surface area and pore volume of various samples.

| Sample | Surface area ($m^2$ $g^{-1}$) | Pore volume ($cm^3$ $g^{-1}$) |
|---|---|---|
| Co/$Co_9S_8$@CNTs-800 | 103.3 | 0.13 |
| Co/$Co_9S_8$@CNTs-900 | 228.8 | 0.35 |
| Co/$Co_9S_8$@CNTs-1000 | 265.3 | 0.39 |

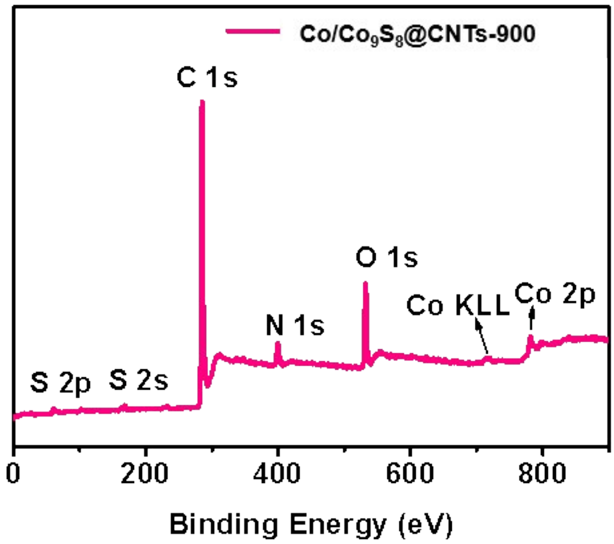


**Figure S9.** XPS survey spectrum of Co/$Co_9S_8$@CNTs-900.

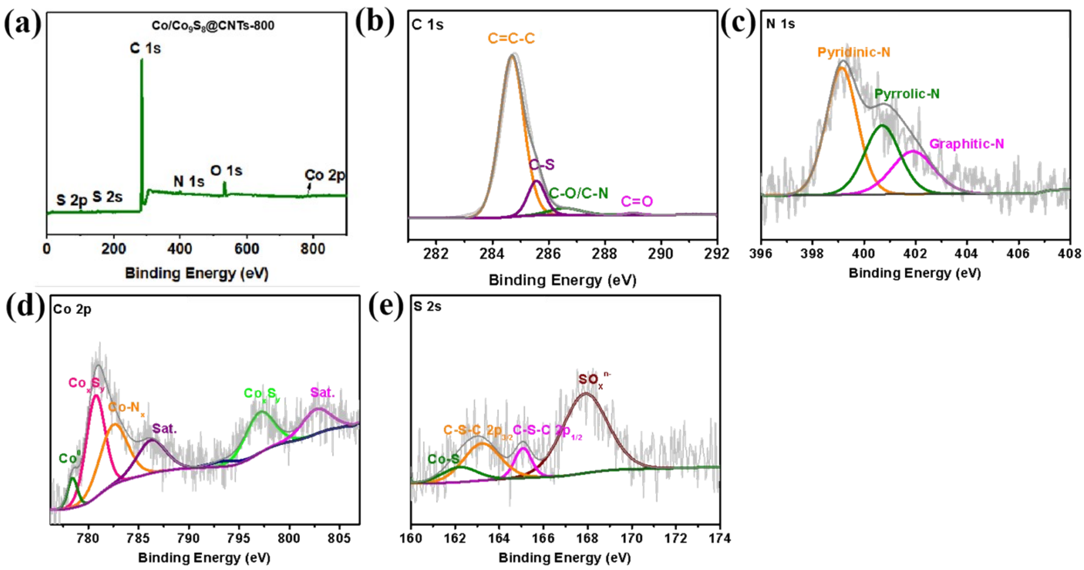


**Figure S10.** (a) XPS survey spectrum of Co/$Co_9S_8$@CNTs-800. High-resolution spectrum of (b) C 1s, (c) N 1s, (d) Co 2p, and (e) S 2p for $Co/Co_9S_8$@CNTs-800.

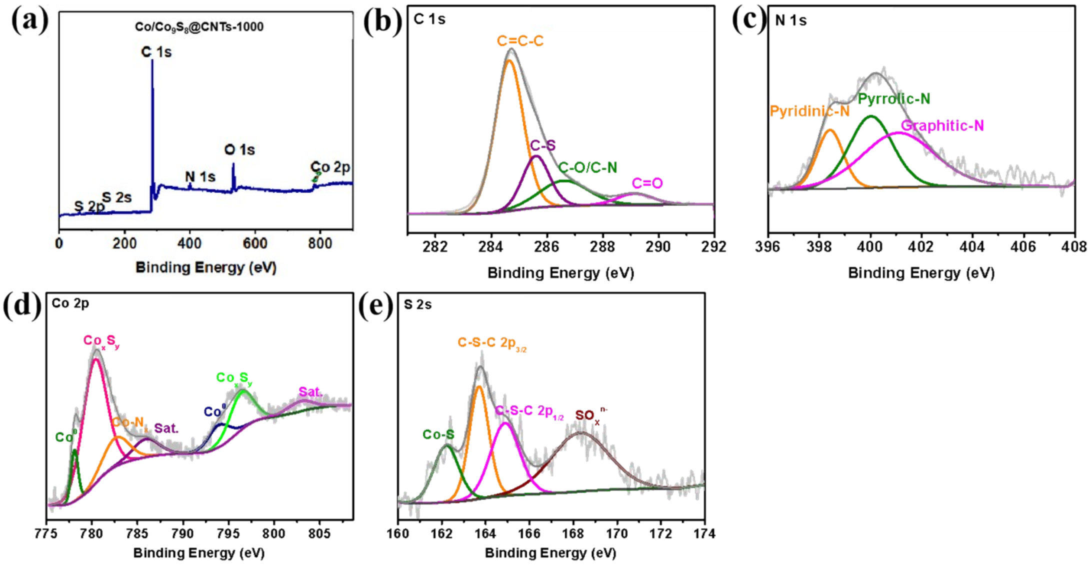


**Figure S11.** (a) XPS survey spectrum of $Co/Co_9S_8$@CNTs-1000. High-resolution spectrum of (b) C 1s, (c) N 1s, (d) Co 2p and (e) S 2p for $Co/Co_9S_8$@CNTs-1000.

**Table S2.** Surface elemental contents in various samples from XPS survey spectrum.

| | C | N | O | S | Co |
|---|---|---|---|---|---|
| $Co/Co_9S_8$@CNTs-800 | 92.56 | 1.39 | 5.53 | 0.19 | 0.32 |
| $Co/Co_9S_8$@CNTs-900 | 80.94 | 5.25 | 11.38 | 1.15 | 1.27 |
| $Co/Co_9S_8$@CNTs-1000 | 86.26 | 3.26 | 8.98 | 0.79 | 0.71 |

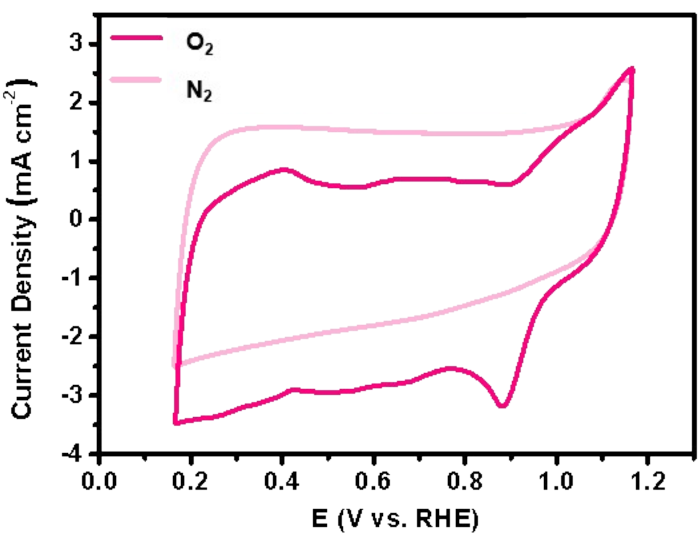


**Figure S12.** CV curves of Co/$Co_9S_8$@CNTs-900 in $O_2$- and $N_2$-saturated 0.1 M KOH solution with a sweep rate of 50 mV $s^{-1}$.

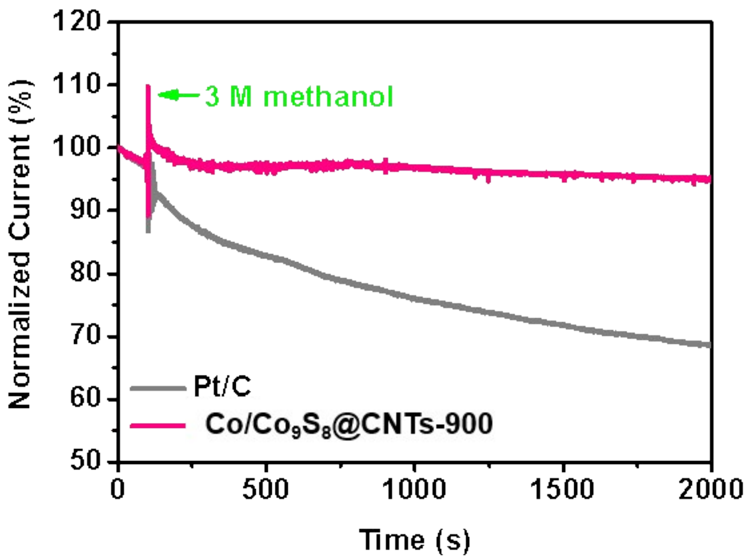


**Figure S13.** Methanol crossover tests for Co/$Co_9S_8$@CNTs-900 and 20 wt% Pt/C catalyst by adding 3 M methanol into the electrolyte at 100 s.

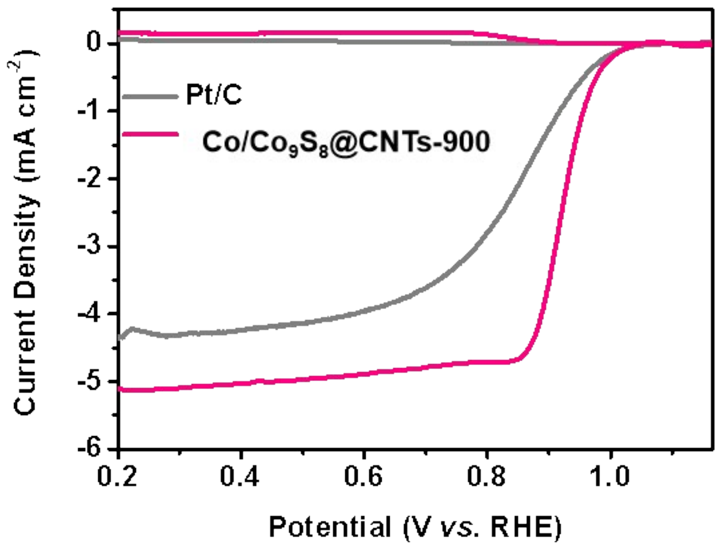


**Figure S14.** RRDE curves of Co/Co$_9$S$_8$@CNTs-900 and 20 wt% Pt/C.

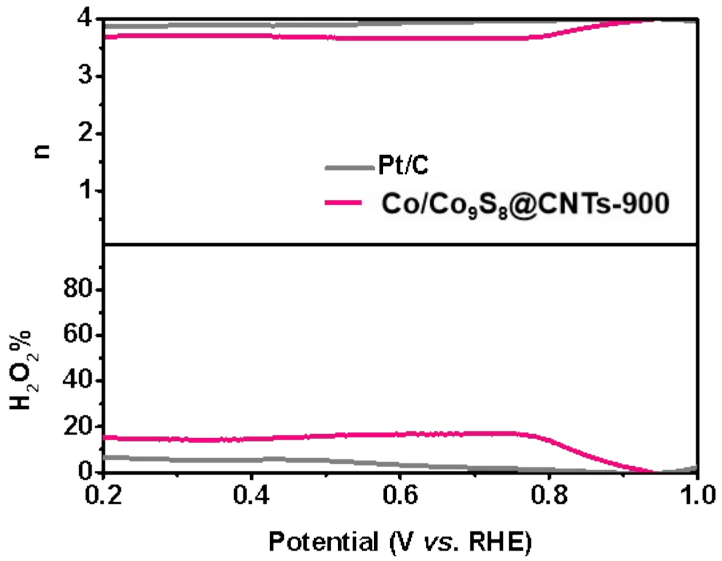


**Figure S15.** The number of transfer electrons (n) and $H_2O_2$ yield plots of Co/Co$_9$S$_8$@CNTs-900 and 20 wt% Pt/C from 0.2 V to 0.9 V (vs. RHE).

**Table S3.** The comparison of catalytic performances for ORR in 0.1 M KOH between Co/Co$_9$S$_8$@CNTs-900 and other Co-based materials reported in the literature.

| Catalysts | Catalyst loading (mg cm$^{-2}$) | $E_{1/2}$ (V vs. RHE) | limiting current density | Tafel slope (mV dec$^{-1}$ ) | Ref. |
|---|---|---|---|---|---|
| Co/Co$_9$S$_8$@CNTs-900 | 0.40 | 0.925 | 5.106 | 48 | This work |
| Co/Co$_9$S$_8$@CNTs-800 | 0.40 | 0.895 | 4.24 | 123 | This work |

| | | | | | |
|---|---|---|---|---|---|
| **Co/$Co_9S_8$@CNTs-1000** | **0.40** | **0.907** | **5.25** | **85** | **This work** |
| Co/CNFs (1000) | -- | 0.896 | -- | 73 | Ref. 1 |
| Co-$Co_9S_8$@SN-CNTs-900 | 0.40 | 0.810 | ---- | -- | Ref. 2 |
| $Co_2P$/CoN-in-NCNTs | 0.10 | 0.850 | 5.01 | 49 | Ref. 3 |
| Co@N-CNTF-2 | 0.28 | 0.810 | -- | 47.6 | Ref. 4 |
| CF-NG-Co | 0.28 | 0.88 | 5.5 | 44 | Ref. 5 |
| Co/CoP-HNC | 0.19 | 0.83 | -- | 59.4 | Ref. 6 |
| NS/rGO-Co2 | 0.485 | 0.84 | 5.964 | 52 | Ref. 7 |
| $Co_3O_4$/NCMTs | 0.28 | 0.778 | 4.5 | 42.9 | Ref. 8 |
| $Co_3O_4$-PPy/GN | 0.20 | 0.77 | 4.471 | -- | Ref. 9 |
| $Co_9S_8$-NSHPCNF | 0.30 | 0.82 | 4.81 | 65 | Ref. 10 |
| Co9S8/CD@NSC | 0.249 | 0.84 | -- | 76.2 | Ref. 11 |
| OSHs-NSC-$Co_9S_8$ | 0.194 | 0.82 | 5.35 | -- | Ref. 12 |

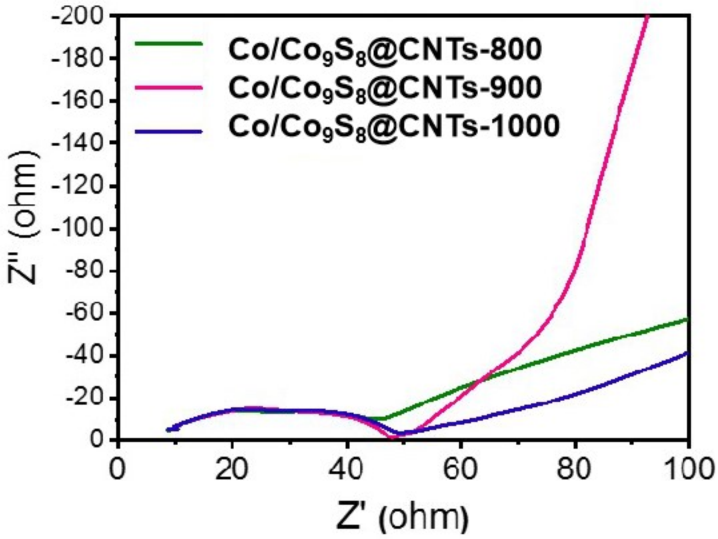


**Figure S16.** The electrochemical impedance spectroscopy of as-prepared Co/$Co_9S_8$@CNTs.

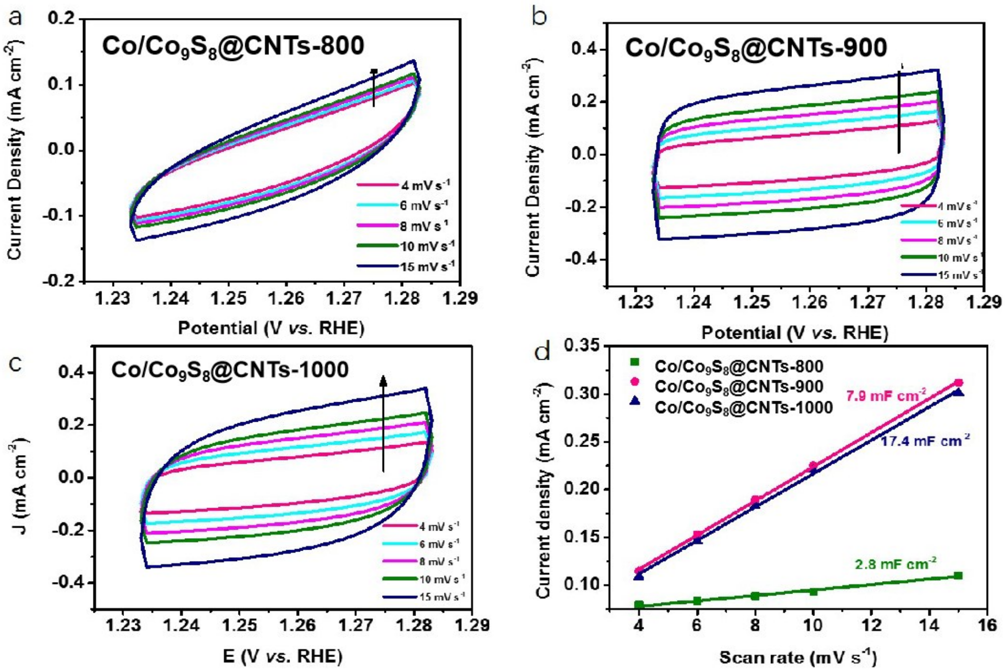


**Figure S17.** Cyclic voltammograms curves for **a)** $Co/Co_9S_8$@CNTs-800, **b)** $Co/Co_9S_8$@CNTs-900, **c)** $Co/Co_9S_8$@CNTs-1000 in the region of 1.233 ~1.283 V vs. RHE at various scan rates. **d)** The electrochemical double-layer capacitances ($C_{dll}$) of various samples.

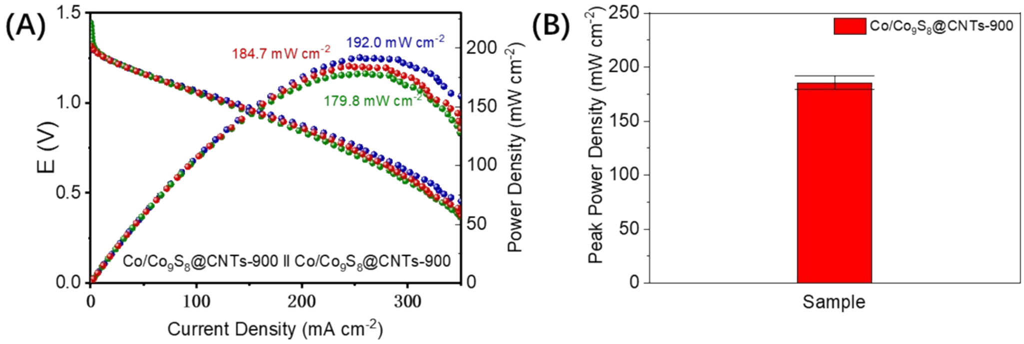


**Figure S18.** (**A)** The discharging LSV curve tests of Zn-air batteries with Co/$Co_9S_8$@CNTs-900. (**B)** The peak power density of Zn-air batteries with Co/$Co_9S_8$@CNTs-900.

# Reference：

1. Yang, Z.; Zhao, C.; Qu, Y.; Zhou, H.; Zhou, F.; Wang, J.; Wu, Y.; Li, Y., Trifunctional Self-Supporting Cobalt-Embedded Carbon Nanotube Films for ORR, OER, and HER Triggered by Solid Diffusion from Bulk Metal. *Adv. Mater.* **2019,** *31* (12), 1808043.

2. Han, H.; Bai, Z.; Zhang, T.; Wang, X.; Yang, X.; Ma, X.; Zhang, Y.; Yang, L.; Lu, J., Hierarchical design and development of nanostructured trifunctional catalysts for electrochemical oxygen and hydrogen reactions. *Nano Energy* **2019,** *56*, 724-732.

3. Guo, Y.; Yuan, P.; Zhang, J.; Xia, H.; Cheng, F.; Zhou, M.; Li, J.; Qiao, Y.; Mu, S.; Xu, Q., Co2P–CoN Double Active Centers Confined in N-Doped Carbon Nanotube: Heterostructural Engineering for Trifunctional Catalysis toward HER, ORR, OER, and Zn–Air Batteries Driven Water Splitting. *Adv. Funct. Mater.* **2018,** *28* (51), 1805641.

4. Guo, H.; Feng, Q.; Zhu, J.; Xu, J.; Li, Q.; Liu, S.; Xu, K.; Zhang, C.; Liu, T., Cobalt nanoparticle-embedded nitrogen-doped carbon/carbon nanotube frameworks derived from a metal–organic framework for tri-functional ORR, OER and HER electrocatalysis. *J Mater. Chem. A* **2019,** *7* (8), 3664-3672.

5. Pei, Z.; Tang, Z.; Liu, Z.; Huang, Y.; Wang, Y.; Li, H.; Xue, Q.; Zhu, M.; Tang, D.; Zhi, C., Construction of a hierarchical 3D Co/N-carbon electrocatalyst for efficient oxygen reduction and overall water splitting. *J Mater. Chem. A* **2018,** *6* (2), 489-497.

6. Hao, Y.; Xu, Y.; Liu, W.; Sun, X., Co/CoP embedded in a hairy nitrogen-doped carbon polyhedron as an advanced tri-functional electrocatalyst. *Materials Horizons*

**2018,** *5* (1), 108-115.

7. Wang, N.; Li, L.; Zhao, D.; Kang, X.; Tang, Z.; Chen, S., Graphene Composites with Cobalt Sulfide: Efficient Trifunctional Electrocatalysts for Oxygen Reversible Catalysis and Hydrogen Production in the Same Electrolyte. *Small* **2017,** *13* (33), 1701025.

8. Wang, B.; Xu, L.; Liu, G.; Zhang, P.; Zhu, W.; Xia, J.; Li, H., Biomass willow catkin-derived Co3O4/N-doped hollow hierarchical porous carbon microtubes as an effective tri-functional electrocatalyst. *J Mater. Chem. A* **2017,** *5* (38), 20170-20179.

9. Ren, G.; Li, Y.; Guo, Z.; Xiao, G.; Zhu, Y.; Dai, L.; Jiang, L., A bio-inspired Co3O4-polypyrrole-graphene complex as an efficient oxygen reduction catalyst in one-step ball milling. *Nano Research* **2015,** *8* (11), 3461-3471.

10. Peng, W.; Wang, Y.; Yang, X.; Mao, L.; Jin, J.; Yang, S.; Fu, K.; Li, G., Co9S8 nanoparticles embedded in multiple doped and electrospun hollow carbon nanofibers as bifunctional oxygen electrocatalysts for rechargeable zinc-air battery. *Applied Catalysis B: Environmental* **2020,** *268*, 118437.

11. Zhang, P.; Bin, D.; Wei, J.-S.; Niu, X.-Q.; Chen, X.-B.; Xia, Y.-Y.; Xiong, H.-M., Efficient Oxygen Electrocatalyst for Zn–Air Batteries: Carbon Dots and Co9S8 Nanoparticles in a N,S-Codoped Carbon Matrix. *ACS Appl. Mater. Inter.* **2019,** *11* (15), 14085-14094.

12. Tang, K.; Yuan, C.; Xiong, Y.; Hu, H.; Wu, M., Inverse-opal-structured hybrids of N, S-codoped-carbon-confined Co9S8 nanoparticles as bifunctional oxygen electrocatalyst for on-chip all-solid-state rechargeable Zn-air batteries. *Applied*

*Catalysis B: Environmental* **2020,** *260*, 118209.